



Spin motive force by the momentum-space Berry phase in magnetic Weyl semimetals

Akira Harada  and Hiroaki Ishizuka 

Department of Physics, Tokyo Institute of Technology, Meguro, Tokyo 152-8551, Japan



(Received 7 February 2022; revised 8 April 2023; accepted 13 April 2023; published 5 May 2023)

We show that the magnetic precession of ferromagnetic moments in a noncentrosymmetric magnetic Weyl semimetal induces a dc electric current through a mechanism analogous to an adiabatic charge pump. The dc current is a consequence of a Berry phase effect in momentum space resulting from the circular motion of Weyl nodes induced by the precession. This mechanism resembles the Faraday effect, namely, an induced magnetic field by a circular electric current. The circular motion of Weyl nodes induces a magnetic charge current in momentum space, which results in a Berry phase that describes the adiabatic pump. Experimentally, this phenomenon is similar to a spin motive force, which is an electric current induced by magnetic precession in the presence of the spatial gradient of magnetization. However, unlike a conventional spin motive force, this dc current occurs without the magnetization gradient. The result demonstrates a nontrivial interplay between the topological electronic state and magnetic dynamics.

DOI: [10.1103/PhysRevB.107.195202](https://doi.org/10.1103/PhysRevB.107.195202)

I. INTRODUCTION

The interplay of topological electronic states and magnetism realizes peculiar electronic states and phenomena arising from the interplay, which attract attention from both basic science and applications such as spintronics [1]. For instance, in topological insulators [2,3], coupling the edge mode to a ferromagnet makes it a quantum anomalous Hall insulator [4–6], and coupling topological insulators to antiferromagnets is a route to realize an axion insulator [7]. The effect of magnetism on nontrivial electronic states was also studied in relation to Weyl semimetals (WSMs) [8–12] such as in pyrochlore iridates [11,13,14]. In these materials, their transport properties were discussed in relation to Weyl electrons, such as a relatively large Hall effect with small magnetization [15–17], and a nonmonotonic magnetic-field dependence of the anomalous Hall effect in EuTiO_3 [18]. Understanding the effect of coupling between the magnetic order and the topological electronic states was key to understanding these phenomena.

On the other hand, the dynamical or optical properties of magnetic materials bring about rich functionalities [19–22], the study of which has been one of the major topics in spintronics. While many studies were done on the effect of magnetic textures, much less is known about the role of the topological/geometrical nature of electron bands on the dynamical properties. In this paper, we study the electrical response of WSMs due to the magnetic dynamics as an illustration of the interplay, in which we find an electrical current analogous to an adiabatic charge pump [23,24] driven by the precession of the magnetic moment.

A quantity that plays a central role in this study is the momentum-space Berry phase defined by $\mathbf{b}_{kn} = \nabla_{\mathbf{k}} \times \mathbf{a}_{kn}$, where $\mathbf{a}_{kn} = -i\langle u_{nk} | \nabla_{\mathbf{k}} | u_{nk} \rangle$ is the Berry connection with $|u_{nk}\rangle$ being the Bloch function of the n th band with momentum \mathbf{k} and $\nabla_{\mathbf{k}} = (\partial_{k_x}, \partial_{k_y}, \partial_{k_z})$ [25,26]. The Berry curvature is directly related to the topological nature of electronic states

such as the Hall conductivity in quantum [27] and anomalous Hall effects [28].

Another system with a characteristic feature in \mathbf{b}_{kn} is the WSM, where the Weyl node is a singular point of the Berry curvature with $\mathbf{b}_{kn} \propto (\mathbf{k} - \mathbf{k}_0)/|\mathbf{k} - \mathbf{k}_0|^3$ (\mathbf{k}_0 is the position of the Weyl node). The distribution of \mathbf{b}_{kn} resembles that of the magnetic field around a point magnetic charge, hence sometimes called a magnetic monopole in momentum space. The divergent Berry curvature at the Weyl node is often related to the unique properties of WSMs. For instance, it gives rise to the nonmonotonic magnetization dependence of anomalous Hall conductance [18] and enhances the electromagnetic response related to Berry curvature as in anomaly-related magnetoresistance [29]. The latter is generally possible in a system with a finite Berry curvature, but the large Berry curvature around the Weyl nodes enhances the phenomenon [30,31]. The enhancement of the Berry phase effect makes the WSM an interesting material for studying the Berry-phase-related phenomena.

Besides the Berry curvature in momentum space \mathbf{b}_{kn} , a Berry curvature with a time derivative

$$\mathbf{e}_{kn}(t) = \partial_t \mathbf{a}_{kn}(t) - \nabla_{\mathbf{k}} a_{kn}^t(t) \quad (1)$$

also contributes to electron transport in a system where the Hamiltonian $H(t)$ evolves slowly over time, a phenomenon known as an adiabatic pump [23,24]. Here, $\mathbf{a}_{kn}(t) = -i\langle u_{nk}(t) | \nabla_{\mathbf{k}} | u_{nk}(t) \rangle$ is the Berry connection defined by the Bloch function for the instantaneous Hamiltonian $H(t)$ and $a_{kn}^t(t) = -i\langle u_{nk}(t) | \partial_t | u_{nk}(t) \rangle$. However, the charge pump requires a time-dependent perturbation comparable to the bandwidth, and hence it is realized only in cold atoms [32,33]. An exception to the obstruction might be the WSM, in which the divergent Berry curvature near the Weyl nodes enhances the $\mathbf{e}_{kn}(t)$ field [34,35].

As a demonstration of the impact of $\mathbf{e}_{kn}(t)$ induced by the magnetic dynamics, we study the Larmor precession of a ferromagnetic moment in a magnetic WSM. We show that

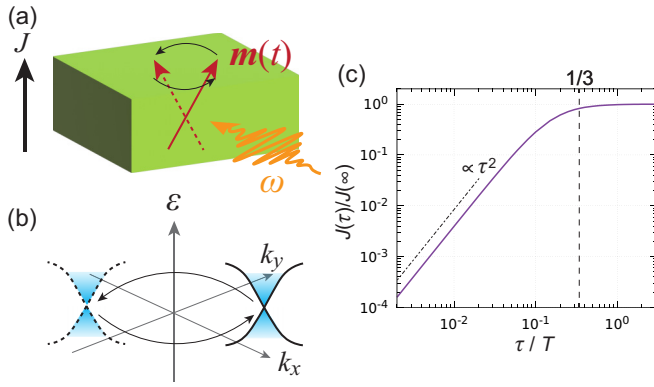


FIG. 1. Adiabatic charge pumping and spin motive force. (a) Schematic of the magnetic resonance. The charge current flows along the direction of the uniform moment (z axis in the main text). (b) Displacement of Weyl nodes by the precession of the magnetic moment. The Weyl nodes shown by the solid (dotted) lines correspond to those for the magnetization in (a) shown by the arrow with the solid (dotted) line. Upon magnetic precession, the Weyl node moves in momentum space following $\mathbf{m}(t)$. (c) The relaxation-time dependence of the induced charge current by one node. The result is obtained by numerically integrating Eq. (8). The result is for $\mu/v = 1$, $v_0/v = 0.1$, and $J_K m_\perp/v = 0.1$.

$e_{kn}(t)$ induced by the precession causes an electric current J along the magnetization direction. By explicit calculation, we show $J \propto \tau^2$ dependence when the relaxation time τ is short, whereas it saturates above $\tau \sim T/3$ where T is the period of the precession [Fig. 1(c)]. The saturation is a manifestation of the dissipationless current. The low crossover τ/T implies that the long τ regime is experimentally accessible in a clean WSM if T is in picoseconds. These features are experimentally testable in noncentrosymmetric magnetic WSMs [36–41]. The results demonstrate a unique transport phenomenon arising from topological electronic states and magnetic dynamics.

II. MODEL AND METHOD

A. Weyl Hamiltonian

For concreteness, we consider noncentrosymmetric Weyl semimetals coupled to a ferromagnetic moment. The effective Hamiltonian for these materials is given by a set of Weyl Hamiltonians [8, 12], each reading

$$H(t) = \sum_{\mathbf{k}, \alpha, \beta} c_{k\alpha}^\dagger [v\mathbf{k} \cdot \boldsymbol{\sigma} - \{v_0 k_z + \mu(t)\} \delta_{\alpha\beta} - J_K \mathbf{m}(t) \cdot \boldsymbol{\sigma}]_{\alpha\beta} c_{k\beta}, \quad (2)$$

where $\boldsymbol{\sigma} = (\sigma^x, \sigma^y, \sigma^z)$ ($\sigma^{x,y,z}$ are the Pauli matrices), μ_0 is the chemical potential at equilibrium, v is the velocity of the Weyl electron, v_0 ($|v_0| < |v|$) is the velocity of the tilting term, J_K is the Kondo coupling, $c_{k\alpha}$ ($c_{k\alpha}^\dagger$) is the annihilation (creation) operator of an electron with momentum $\mathbf{k} = (k_x, k_y, k_z)$, and $\mathbf{m}(t) = [m_x(t), m_y(t), m_z(t)]$ ($|\mathbf{m}(t)| = 1$) is a unit vector parallel to the ferromagnetic moment. Hereon, we take $\hbar = a = 1$. The time dependence of $\mu(t)$ is a consequence of the magnetic dynamics, which we discuss later. This model

is often used as an effective model for WSMs with the Fermi level near the Weyl node.

The Larmor precession of the magnetic moment about the z axis is given by

$$\mathbf{m}(t) = (m_\perp \sin(\omega t), m_\perp \cos(\omega t), \sqrt{1 - m_\perp^2}), \quad (3)$$

where m_\perp is the amplitude of precession and $\omega = 2\pi/T$ is the frequency. For the Hamiltonian in Eq. (2), the dynamics of magnetic moments shift the position of Weyl nodes in momentum space. This is a consequence of band deformation by magnetism similar to those generally seen in magnetic WSMs [14–16, 18]. The steady precession of ferromagnetic moments occurs, for example, in ferromagnetic resonance, as we will discuss later.

B. Semiclassical Boltzmann theory

We use the semiclassical Boltzmann theory [26] to study the charge transport under the precession of the moment. Within the relaxation-time approximation, the Boltzmann equation reads

$$\partial_t f_{kn}(t) = -\frac{1}{\tau} [f_{kn}(t) - f_{kn}^0(t)], \quad (4)$$

where τ is the relaxation time, $f_{kn}(t)$ is the average density of electron with momentum \mathbf{k} and band index n at the time t , and $f_{kn}^0(t) = 1/(e^{\beta[\varepsilon_{kn}(t) - \mu(t)]} + 1)$ is the Fermi distribution function for the instantaneous Hamiltonian $H(t)$. Here, $\mu(t)$ is defined so that the electron density for the instantaneous Hamiltonian $N = \int \frac{d^3k}{(2\pi)^3} f_{kn}^0(t)$ is conserved.

The formal solution to Eq. (4) reads

$$\begin{aligned} f_{kn}(t) &= f_{kn}^0(t) e^{-\frac{t-t_0}{\tau}} + \int_{t_0}^t \frac{dt'}{\tau} e^{-\frac{t-t'}{\tau}} f_{kn}^0(t'), \\ &= \int_0^\infty \frac{dt'}{\tau} e^{-\frac{t-t'}{\tau}} f_{kn}^0(t-t'), \end{aligned} \quad (5)$$

where t_0 is the initial time; we assume that the electrons are in equilibrium at t_0 . In the second line, we assumed $t_0/\tau \rightarrow -\infty$. For a periodically driven system with period $T = 2\pi/\omega$, Eq. (5) becomes

$$f_{kn}(t) = \frac{1}{1 - e^{-\frac{T}{\tau}}} \int_0^T \frac{dt'}{\tau} e^{-\frac{t-t'}{\tau}} f_{kn}^0(t-t'), \quad (6)$$

as $f_{kn}^0(t) = f_{kn}^0(t+T)$.

Within the Boltzmann theory, the electric current produced by adiabatic pumping reads [26]

$$\mathbf{J}(t) = \sum_n \int \frac{d^3k}{(2\pi)^3} q \mathbf{e}_{kn}(t) f_{kn}(t), \quad (7)$$

where q is the charge of the carrier, and the sum over n is for all bands in the system. Combining this formula and Eq. (5), the average current in a periodically driven system reads

$$\bar{\mathbf{J}} = \sum_n \int \frac{d^3k}{(2\pi)^3} \int_0^T \frac{dt}{T} \int_0^T \frac{dt'}{\tau} \frac{q e^{-\frac{t-t'}{\tau}}}{1 - e^{-\frac{T}{\tau}}} \mathbf{e}_{kn}(t) f_{kn}(t-t'). \quad (8)$$

In the following, we assume the Fermi distribution for zero temperature. Similar to adiabatic pumping, the thermal fluctuation gives a small correction to the zero-temperature result,

because all electrons in the Fermi surface contribute to the current. Hence, the result should be valid even at a finite temperature as long as the temperature is small compared to the chemical potential.

III. RESULTS

A. $\tau/T \ll 1$ case

When $\tau/T \ll 1$, Eq. (8) becomes [42]

$$\bar{\mathbf{J}} \sim \int_0^T \frac{dt}{T} \int_D \frac{d^3k}{(2\pi)^3} \mathbf{e}_{\mathbf{k}+J_K \mathbf{m}(t) - \tau J_K \dot{\mathbf{m}}(t) + \tau^2 J_K \ddot{\mathbf{m}}(t), n(t)} + O(J_K^3). \quad (9)$$

Here, D is the region inside the Fermi surface. To the second order in J_K , the average current produced by Eq. (3) reads

$$\bar{\mathbf{J}} = \left[0, 0, -\text{sgn}(v) \frac{q\tau^2 \omega^3}{12\pi^2} F(v_0/v) \left(\frac{J_K m_\perp}{v} \right)^2 \right], \quad (10)$$

$$F(x) = 1 + 3 \left(\frac{1}{x^2} - 1 \right) \left[1 - \frac{\text{atanh}(x)}{x} \right]. \quad (11)$$

The $\text{sgn}(v)$ in the equation reflects the chirality of the Weyl node. We note that the current does not depend on the chemical potential despite finite doping [42]. Hence, a finite current flows by a mechanism similar to the adiabatic pump.

In a recent work, the noticeable contribution of the adiabatic pump in a WSM was discussed using an analogy to electromagnetic induction. When a circular electric current flows, it produces the magnetic field penetrating the circuit known as Ampère's law. Similarly, if a magnetic charge exists, the current of magnetic charges induces an electric field as described by an extension of Faraday's law. This analogy also works for Weyl electrons, in which the distribution of the $\mathbf{e}_{\mathbf{k}n}(t)$ field by the circular motion of Weyl nodes (a magnetic monopole of Berry curvature $\mathbf{b}_{\mathbf{k}n}$) resembles that of the magnetic field induced by the circular electric current [35]. This argument also applies to our setup where the position of the Weyl point is given by $\mathbf{k}_0 = J_K \mathbf{m}(t)/v$. However, we expect a stronger current in our setup than the previous proposal because the Kondo coupling is typically stronger than the coupling to electromagnetic fields.

The current produced by this mechanism is sensitive to the magnetization direction while it is inert to the direction of incident light. In the magnetoresonance experiment, the incident microwave from any direction induces the same magnetic precession as long as the magnetic field component is perpendicular to the magnetization. As the origin of the above current is a consequence of the coupling to the magnetic moment, any incident light producing the same precession should produce the same result. On the other hand, the magnetization direction affects the result because the plane of precession changes. The sensitivity of electric current to the magnetization direction, rather than to the incident light, provides a way to delineate the microscopic origin of the current.

We note that this current is a different phenomenon from the conventional spin motive force (SMF) [43–45]. In SMF, the electric current flows in the presence of both magnetic precession and the gradient of magnetization. Intuitively, this phenomenon is often interpreted as a consequence of a fictitious electric field induced by the magnetization dynamics

or the Berry phase in real space. In contrast, the current in Eq. (10) is related to the momentum-space Berry phase.

B. $\tau/T \gg 1$ limit

We next consider the long relaxation-time limit $\tau/T \gg 1$. In this limit, the average current reads

$$\bar{\mathbf{J}} = \int_0^T \frac{dt' dt}{T^2} \mathbf{e}_{\mathbf{k}(t') f_{\mathbf{k}n}^0(t')}. \quad (12)$$

To the second order in J_K , it is

$$\bar{\mathbf{J}} = \left[0, 0, -\text{sgn}(v) \frac{q\omega}{12\pi^2} F(v_0/v) \left(\frac{J_K m_\perp}{v} \right)^2 \right], \quad (13)$$

where $F(x)$ is in Eq. (11). This formula is essentially equivalent to the $\tau/|t - t_0| \gg 1$ case studied previously in Ref. [35]. In Eq. (13), the current is linearly proportional to ω , resembling the quantization of pumped charges in the adiabatic pump.

Note that, in this limit, the current does not depend on τ . Compared to the $\tau/T \ll 1$ case, the current simply differs by a factor of $(\omega\tau)^2$. The result implies that the current, which increases with $(\omega\tau)^2$ in the small τ/T regime, saturates as it approaches $\tau\omega = 1$. Therefore, we expect a crossover between the $\tau/T \ll 1$ and $\tau/T \gg 1$ regimes at $\tau \sim T$.

C. Numerical calculation

To further investigate the τ dependence, we numerically evaluated the τ dependence of Eq. (8). Figure 1(c) is the result for the $\mu/v = 1$, $v_0/v = 0.1$, and $J_K m_\perp/v = 0.1$ case. The numerical result (solid line) is proportional to τ^2 in the small τ/T limit and saturates to a constant at around $\tau/T \gtrsim 1/3$. It is semiquantitatively consistent with the above argument where the crossover occurs at $\tau\omega = 2\pi\tau/T \sim 1$. In the experiment, the magnetic resonance frequency ranges between 10^9 and 10^{12} s⁻¹ while the relaxation time is in 10^{-15} – 10^{-12} s. Hence, the adiabatic regime $\tau/T \gg 1$ might also be relevant to the experiment.

D. Magnitude of current density

We next turn to the magnitude of current expected in a magnetic WSM. To evaluate the magnitude, we need to know the amplitude of the magnetic precession. The dynamics of the ferromagnetic moment is described by the Landau-Lifshitz-Gilbert equation,

$$\partial_t \mathbf{m}(t) = -\gamma \mathbf{m}(t) \times \mathbf{B}(t) + \alpha \mathbf{m}(t) \times \partial_t \mathbf{m}(t), \quad (14)$$

where γ is the gyromagnetic constant, α is the Gilbert damping constant [46,47], and $\mathbf{B}(t) = [B_x(t), B_y(t), B_z]$; we assume the static magnetic field is along the z axis. Suppose the incident microwave is $B_x(t) = B_x^0 \cos(\omega t)$ and $B_y(t) = 0$. Then, at the magnetic resonance frequency $\omega = \pm\gamma B_z$, the approximate solution of Eq. (14) assuming $m_z(t) \sim 1$ reads

$$m_x(t) = \frac{B_x^0}{\alpha B_z} \sin(\omega t), \quad m_y(t) = \frac{B_x^0}{\alpha B_z} \cos(\omega t). \quad (15)$$

Hence, the amplitude of magnetic precession is $m_\perp = B_x^0/\alpha B_z$.

We estimate the induced current using Eq. (10) and the above result. For the case $v = 10^5 \text{ ms}^{-1}$, $v_0 = 10^4 \text{ ms}^{-1}$, $J_K = 10 \text{ meV}$, $\tau = 10^{-12} \text{ s}$, $B_x^0 = 10^{-5} \text{ T}$, $B_z = 10^{-1} \text{ T}$, and $\alpha = 10^{-3}$, the current density reads $J \sim 10^{-3} \text{ mA cm}^{-2}$. This estimate is several orders of magnitude larger compared to the photocurrent by a similar mechanism [34,35], despite the orders-of-magnitude smaller frequency $\omega/2\pi \sim 2.8 \text{ GHz}$. Intuitively, the larger current is ascribed to the faster motion of Weyl nodes associated with the larger orbital radius. Using the analogy to classical electromagnetism discussed above, the induced e_{kn} field is larger for Weyl nodes moving at a higher speed. For a fixed frequency, the Weyl nodes move faster for a larger radius of Weyl nodes, hence producing a larger e_{kn} field that results in a larger current.

We also note that linearly polarized electromagnetic waves can induce a finite current, in contrast to the bulk photovoltaic effects in WSM. Recent theories for the bulk photovoltaic effect in a WSM [34,48–50] find that the electric current is sensitive to the polarization of the incident light. In particular, a circularly polarized light is often necessary for a finite photocurrent. This is also the case for a nonlinear Hall effect [58,59]. In contrast, the above argument on magnetic precession assumes a linearly polarized microwave; the circular motion of Weyl nodes is a consequence of the precession of magnetic moment induced by the microwave. The insensitivity to the polarization of incident light distinguishes this phenomenon from the photovoltaic effects [51].

IV. WEYL SEMIMETALS WITH MULTIPLE WEYL NODES

Real materials with Weyl electrons have multiple Weyl nodes, which is partly a manifestation of Nielsen-Ninomiya's theorem [52–54] and in part a consequence of the symmetry requirement. A noncentrosymmetric Weyl semimetal often hosts more than ten Weyl nodes, where the Weyl nodes with the same chirality are the time-reversal pair. Therefore, the current by a pair will be twice that by a Weyl node. With multiple pairs, the induced electric current is the sum of the contribution from all nodes. However, in general, the total current should remain finite.

In special cases, the summation may result in a vanishing current, such as in a WSM with spatial-inversion symmetry. In a WSM with inversion symmetry, two nodes with opposite chirality always appear as a pair; if one node exists at wave number k_0 , then its pair node is at $-k_0$. As the current in Eqs. (10) and (13) depends on the chirality manifested in $\text{sgn}(v)$, the contribution from two nodes cancels. This argument holds for a WSM with $2n$ nodes because each pair gives zero current. Hence, the current vanishes in centrosymmetric WSMs.

The absence of electric current in a centrosymmetric WSM is a consequence of the symmetry restriction on the response tensors. Phenomenologically, the phenomenon studied here is a nonlinear response to the ac magnetic field $\bar{J} = \sigma(B_x^0)^2$, where σ is the nonlinear conductivity. With the inversion operation, the current and the magnetic field transform as $\bar{J} \rightarrow -\bar{J}$ and $B_x^0 \rightarrow B_x^0$, respectively. Hence, the phenomeno-

logical formula reads $\bar{J} = -\sigma(B_x^0)^2$, implying $\sigma = -\sigma$, and hence $\sigma = 0$. Therefore, a noncentrosymmetric WSM is necessary for a finite current.

The inversion symmetry is a special symmetry in the way that it restricts all response tensors. Other symmetries, such as mirror symmetry, make certain components of the tensors vanish. However, they do not restrict all tensor components, similar to the arguments for the photovoltaic effect.

V. DISCUSSIONS

In this paper, we studied the electric current induced by the precession of a magnetic moment in a type-I magnetic WSM. We find that the momentum-space Berry curvature induces a current similar to the adiabatic charge pump. The induced current is insensitive to the incident light direction and polarization because it is a consequence of the coupling to the magnetic moment. Instead, it depends on the direction of the magnetic moment as the plane of the precession depends on the direction of the moment. This mechanism gives rise to a finite electric current in a magnetic WSM with a noncentrosymmetric crystal structure. Note that this current is different from the contribution in a field theory [55] or an ac spin motive force [56,57], which predicts an ac response. Finally, our estimate using a typical value for a WSM and a ferromagnet gives $\sim 10^{-3} \text{ mA cm}^{-2}$, which should be observable in the experiments.

The key feature of the Weyl electron in this phenomenon is the degeneracy at the Weyl node, which allows a small perturbation to significantly change the electronic states. Hence, a similar effect is expected in other materials with similar features, such as type-II WSMs.

Experimentally, this phenomenon should be observable using a setup similar to SMF. However, unlike the conventional SMF, the current due to $e_{kn}(t)$ appears without a magnetization gradient, and the current flows along the net magnetization. These features distinguish the $e_{kn}(t)$ -related current from those by the conventional SMF, and also from those by the Berry phase effect [58,59] arising from the direct coupling of electrons to the electric field.

Recent searches for WSMs discovered various materials with Weyl nodes near the Fermi level, both in noncentrosymmetric [60,61] and magnetic materials [11,16,17,36,38,40,62–64]. Some of these materials have both noncentrosymmetric crystal structures and magnetism, such as CeAlSi [36,40] and PrAlGe_{1-x}Si_x [38]. The symmetry-forced cancellation is violated in these materials, allowing a larger class of physics related to Weyl fermions to give observable consequences. The time-dependent Berry phase $e_{kn}(t)$ is one such effect that provides a route to realize nontrivial phenomena arising from the interplay of magnetism and topological electronic states.

ACKNOWLEDGMENTS

We thank K. Burch, F. Tafti, and H. Yang for useful discussions. This work is supported by JSPS KAKENHI (Grants No. JP18H03676 and No. JP19K14649).

- [1] Q. L. He, T. L. Hughes, N. P. Armitage, Y. Tokura, and K. L. Wang, Topological spintronics and magnetoelectronics, *Nat. Mater.* **21**, 15 (2022).
- [2] M. Z. Hasan and C. L. Kane, Colloquium: Topological insulators, *Rev. Mod. Phys.* **82**, 3045 (2010).
- [3] X.-L. Qi and S.-C. Zhang, Topological insulators and superconductors, *Rev. Mod. Phys.* **83**, 1057 (2011).
- [4] C.-Z. Chang, J. Zhang, X. Feng, J. Shen, Z. Zhang, M. Guo, K. Li, Y. Ou, P. Wei, L.-L. Wang, Z.-Q. Ji, Y. Feng, S. Ji, X. Chen, J. Jia, X. Dai, Z. Fang, S.-C. Zhang, K. He, Y. Wang, L. Lu, X.-C. Ma, and Q.-K. Xue, Experimental observation of the quantum anomalous Hall effect in a magnetic topological insulator, *Science* **340**, 167 (2013).
- [5] J. G. Checkelsky *et al.*, Trajectory of the anomalous Hall effect towards the quantized state in a ferromagnetic topological insulator, *Nat. Phys.* **10**, 731 (2014).
- [6] X. Kou *et al.*, Scale-Invariant Quantum Anomalous Hall Effect in Magnetic Topological Insulators beyond the Two-Dimensional Limit, *Phys. Rev. Lett.* **113**, 137201 (2014).
- [7] X.-L. Qi, T. L. Hughes, and S.-C. Zhang, Topological field theory of time-reversal invariant insulators, *Phys. Rev. B* **78**, 195424 (2008).
- [8] B. Yan and C. Felser, Topological materials: Weyl semimetals, *Annu. Rev. Condens. Matter Phys.* **8**, 337 (2017).
- [9] S. Murakami, Phase transition between the quantum spin Hall and insulator phases in 3D: Emergence of a topological gapless phase, *New J. Phys.* **9**, 356 (2007).
- [10] A. A. Burkov and L. Balents, Weyl Semimetal in a Topological Insulator Multilayer, *Phys. Rev. Lett.* **107**, 127205 (2011).
- [11] X. Wan, M. Turner, A. Vishwanath, and S. Y. Savrasov, Topological semimetal and Fermi-arc surface states in the electronic structure of pyrochlore iridates, *Phys. Rev. B* **83**, 205101 (2011).
- [12] N. P. Armitage, E. J. Mele, and A. Vishwanath, Weyl and Dirac semimetals in three-dimensional solids, *Rev. Mod. Phys.* **90**, 015001 (2018).
- [13] W. Witczak-Krempa, G. Chen, Y. B. Kim, and L. Balents, Correlated quantum phenomena in the strong spin-orbit regime, *Annu. Rev. Condens. Matter Phys.* **5**, 57 (2014).
- [14] W. Witczak-Krempa and Y. B. Kim, Topological and magnetic phases of interacting electrons in the pyrochlore iridates, *Phys. Rev. B* **85**, 045124 (2012).
- [15] E.-G. Moon, C. Xu, Y. B. Kim, and L. Balents, Non-Fermi-Liquid and Topological States with Strong Spin-Orbit Coupling, *Phys. Rev. Lett.* **111**, 206401 (2013).
- [16] K. Ueda, R. Kaneko, J. Fujioka, H. Ishizuka, N. Nagaosa, and Y. Tokura, Spontaneous Hall effect in all-in all-out Weyl semimetal of pyrochlore iridates, *Nat. Commun.* **9**, 3032 (2018).
- [17] C. Shekhar *et al.*, Anomalous Hall effect in Weyl semimetal half-Heusler compounds $R\text{PtBi}$ ($R = \text{Gd}$ and Nd), *Proc. Natl. Acad. Sci. USA* **115**, 9140 (2018).
- [18] K. S. Takahashi *et al.*, Anomalous Hall effect derived from multiple Weyl nodes in high-mobility EuTiO_3 films, *Sci. Adv.* **4**, eaar7880 (2018).
- [19] *Spin Current*, edited by S. Maekawa, S. O. Valenzuela, E. Saitoh, and T. Kimura, 2nd ed. (Oxford University Press, Oxford, UK, 2017).
- [20] Y. Araki and K. Nomura, Charge Pumping Induced by Magnetic Texture Dynamics in Weyl Semimetals, *Phys. Rev. Appl.* **10**, 014007 (2018).
- [21] J. D. Hannukainen, Y. Ferreiros, A. Cortijo, and J. H. Bardarson, Axial anomaly generation by domain wall motion in Weyl semimetals *Phys. Rev. B* **102**, 241401(R) (2020).
- [22] J. D. Hannukainen, A. Cortijo, J. H. Bardarson, and Y. Ferreiros, Electric manipulation of domain walls in magnetic Weyl semimetals via the axial anomaly, *SciPost Phys.* **10**, 102 (2021).
- [23] D. J. Thouless, Quantization of particle transport, *Phys. Rev. B* **27**, 6083 (1983).
- [24] Q. Niu and D. J. Thouless, Quantised adiabatic charge transport in the presence of substrate disorder and many-body interaction, *J. Phys. A: Math. Gen.* **17**, 2453 (1984).
- [25] G. Sundaram and Q. Niu, Wave-packet dynamics in slowly perturbed crystals: Gradient corrections and Berry-phase effects, *Phys. Rev. B* **59**, 14915 (1999).
- [26] D. Xiao, M.-C. Chang, and Q. Niu, Berry phase effect in electronic properties, *Rev. Mod. Phys.* **82**, 1959 (2010).
- [27] D. J. Thouless, M. Kohmoto, M. P. Nightingale, and M. den Nijs, Quantized Hall Conductance in a Two-Dimensional Periodic Potential, *Phys. Rev. Lett.* **49**, 405 (1982).
- [28] R. Karplus and J. M. Luttinger, Hall Effect in Ferromagnetics, *Phys. Rev.* **95**, 1154 (1954).
- [29] D. T. Son and B. Z. Spivak, Chiral anomaly and classical negative magnetoresistance of Weyl metals, *Phys. Rev. B* **88**, 104412 (2013).
- [30] H. Ishizuka and N. Nagaosa, Robustness of anomaly-related magnetoresistance in doped Weyl semimetals, *Phys. Rev. B* **99**, 115205 (2019).
- [31] H. Ishizuka and N. Nagaosa, Tilting dependence and anisotropy of anomaly-related magnetoconductance in type-II Weyl semimetals, *Sci. Rep.* **9**, 16149 (2019).
- [32] S. Nakajima, T. Tomita, S. Taie, T. Ichinose, H. Ozawa, L. Wang, M. Troyer, and Y. Takahashi, Topological Thouless pumping of ultracold fermions, *Nat. Phys.* **12**, 296 (2016).
- [33] M. Lohse, C. Schweizer, O. Zilberberg, M. Aidelsburger, and I. Bloch, A Thouless quantum pump with ultracold bosonic atoms in an optical superlattice, *Nat. Phys.* **12**, 350 (2016).
- [34] H. Ishizuka, T. Hayata, M. Ueda, and N. Nagaosa, Emergent Electromagnetic Induction and Adiabatic Charge Pumping in Noncentrosymmetric Weyl Semimetals, *Phys. Rev. Lett.* **117**, 216601 (2016).
- [35] H. Ishizuka, T. Hayata, M. Ueda, and N. Nagaosa, Momentum-space electromagnetic induction in Weyl semimetals, *Phys. Rev. B* **95**, 245211 (2017).
- [36] T. Suzuki, L. Savary, J.-P. Liu, J. W. Lynn, L. Balents, and J. G. Checkelsky, Singular angular magnetoresistance in a magnetic nodal semimetal, *Science* **365**, 377 (2019).
- [37] D. S. Sanchez, G. Chang, I. Belopolski, H. Lu, J.-X. Yin, N. Alidoust, X. Xu, T. A. Cochran, X. Zhang, Y. Bian, S. S. Zhang, Y.-Y. Liu, J. Ma, G. Bian, H. Lin, S.-Y. Xu, S. Jia, and M. Z. Hasan, Observation of Weyl fermions in a magnetic non-centrosymmetric crystal, *Nat. Commun.* **11**, 3356 (2020).
- [38] H.-Y. Yang, B. Singh, B. Lu, C.-Y. Huang, F. Bahrami, W.-C. Chiu, D. Graf, S.-M. Huang, B. Wang, H. Lin, D. Torchinsky, A. Bansil, and F. Tafti, Transition from intrinsic to extrinsic anomalous Hall effect in the ferromagnetic Weyl semimetal $\text{PrAlGe}_{1-x}\text{Si}_x$, *APL Mater.* **8**, 011111 (2020).

- [39] J. Gaudet, H.-Y. Yang, S. Baidya, B. Lu, G. Xu, Y. Zhao, J. A. Rodriguez-Rivera, C. M. Hoffmann, D. E. Graf, D. H. Torchinsky, P. Nikolić, D. Vanderbilt, F. Tafti, and C. L. Broholm, Weyl-mediated helical magnetism in NdAlSi, *Nat. Mater.* **20**, 1650 (2021).
- [40] H.-Y. Yang, B. Singh, J. Gaudet, B. Lu, C.-Y. Huang, W.-C. Chiu, S.-M. Huang, B. Wang, F. Bahrami, B. Xu, J. Franklin, I. Sochnikov, D. E. Graf, G. Xu, Y. Zhao, C. M. Hoffman, H. Lin, D. H. Torchinsky, C. L. Broholm, A. Bansil, and F. Tafti, Noncollinear ferromagnetic Weyl semimetal with anisotropic anomalous Hall effect, *Phys. Rev. B* **103**, 115143 (2021).
- [41] J.-F. Wang, Q.-X. Dong, Z.-P. Guo, M. Lv, Y.-F. Huang, J.-S. Xiang, Z.-A. Ren, Z.-J. Wang, P.-J. Sun, G. Li, and G.-F. Chen, NdAlSi: A magnetic Weyl semimetal candidate with rich magnetic phases and atypical transport properties, *Phys. Rev. B* **105**, 144435 (2022).
- [42] See Supplemental Material at <http://link.aps.org/supplemental/10.1103/PhysRevB.107.195202> for the derivation of the formula and other technical details.
- [43] A. Stern, Berry's Phase, Motive Forces, and Mesoscopic Conductivity, *Phys. Rev. Lett.* **68**, 1022 (1992).
- [44] S. E. Barnes and S. Maekawa, Generalization of Faraday's Law to Include Nonconservative Spin Forces, *Phys. Rev. Lett.* **98**, 246601 (2007).
- [45] K. Tanabe and J.-I. Ohe, Spin-motive force in ferromagnetic and ferrimagnetic materials, *J. Phys. Soc. Jpn.* **90**, 081011 (2021).
- [46] K. Lenz, H. Wende, W. Kuch, K. Baberschke, K. Nagy, and A. Jánossy, Two-magnon scattering and viscous Gilbert damping in ultrathin ferromagnets, *Phys. Rev. B* **73**, 144424 (2006).
- [47] C. Vittoria, S. D. Yoon, and A. Widom, Relaxation mechanism for ordered magnetic materials, *Phys. Rev. B* **81**, 014412 (2010).
- [48] C.-K. Chan, N. H. Lindner, G. Refael, and P. A. Lee, Photocurrents in Weyl semimetals, *Phys. Rev. B* **95**, 041104(R) (2017).
- [49] F. de Juan, A. G. Grushin, T. Morimoto, and J. E. Moore, Quantized circular photogalvanic effect in Weyl semimetals, *Nat. Commun.* **8**, 15995 (2017).
- [50] P. Bhalla, A. H. MacDonald, and D. Culcer, Resonant Photo-voltaic Effect in Doped Magnetic Semiconductors, *Phys. Rev. Lett.* **124**, 087402 (2020).
- [51] B. I. Sturman and V. M. Fridkin, *The Photovoltaic and Photorefractive Effects in Noncentrosymmetric Materials* (Gordon and Breach, Amsterdam, 1992).
- [52] H. B. Nielsen and M. Ninomiya, Absence of neutrinos on a lattice: (I). Proof by homotopy theory, *Nucl. Phys. B* **185**, 20 (1981).
- [53] H. B. Nielsen and M. Ninomiya, No Go Theorem for Regularizing Chiral Fermions, *Phys. Lett. B* **105**, 219 (1981).
- [54] H. B. Nielsen and M. Ninomiya, Absence of neutrinos on a lattice: (II). Intuitive topological proof, *Nucl. Phys. B* **193**, 173 (1981).
- [55] K. Nomura and N. Nagaosa, Electric charging of magnetic textures on the surface of a topological insulator, *Phys. Rev. B* **82**, 161401(R) (2010).
- [56] C.-M. Ryu, Spin Motive Force and Faraday Law for Electrons in Mesoscopic Rings, *Phys. Rev. Lett.* **76**, 968 (1996).
- [57] K.-W. Kim, J.-H. Moon, K.-J. Lee, and H.-W. Lee, Prediction of Giant Spin Motive Force due to Rashba Spin-Orbit Coupling, *Phys. Rev. Lett.* **108**, 217202 (2012).
- [58] J. E. Moore and J. Orenstein, Confinement-Induced Berry Phase and Helicity-Dependent Photocurrents, *Phys. Rev. Lett.* **105**, 026805 (2010).
- [59] I. Sodemann and L. Fu, Quantum Nonlinear Hall Effect Induced by Berry Curvature Dipole in Time-Reversal Invariant Materials, *Phys. Rev. Lett.* **115**, 216806 (2015).
- [60] S.-M. Huang, S.-Y. Xu, I. Belopolski, C.-C. Lee, G. Chang, B. Wang, N. Alidoust, G. Bian, M. Neupane, C. Zhang, S. Jia, A. Bansil, H. Lin, and M. Zahid Hasan, A Weyl Fermion semimetal with surface Fermi arcs in the transition metal monopnictide TaAs class, *Nat. Commun.* **6**, 7373 (2015).
- [61] S.-Y. Xu, I. Belopolski, N. Alidoust, M. Neupane, G. Bian, C. Zhang, R. Sankar, G. Chang, Z. Yuan, C. C. Lee, S.-M. Huang, H. Zheng, J. Ma, D. S. Sanchez, B. Wang, A. Bansil, F. Chou, P. P. Shibayev, H. Lin, S. Jia, and M. Zahid Hasan, Discovery of a Weyl fermion semimetal and topological Fermi arcs, *Science* **349**, 613 (2015).
- [62] I. Belopolski, K. Manna, D. S. Sanchez, G. Chang, B. Ernst, J. Yin, S. S. Zhang, T. Cochran, N. Shumiya, H. Zheng, B. Singh, G. Bian, D. Multer, M. Litskevich, X. Zhou, S.-M. Huang, B. Wang, T.-R. Chang, S.-Y. Xu, A. Bansil, C. Felser, H. Lin, and M. Z. Hasan, Discovery of topological Weyl fermion lines and drumhead surface states in a room temperature magnet, *Science* **365**, 1278 (2019).
- [63] D. F. Liu, A. J. Liang, E. K. Liu, Q. N. Xu, Y. W. Li, C. Chen, D. Pei, W. J. Shi, S. K. Mo, P. Dudin, T. Kim, C. Cacho, G. Li, Y. Sun, L. X. Yang, Z. K. Liu, S. S. P. Parkin, C. Felser, and Y. L. Chen, Magnetic Weyl semimetal phase in a Kagomé crystal, *Science* **365**, 1282 (2019).
- [64] N. Morali, R. Batabyal, P. K. Nag, E. Liu, Q. Xu, Y. Sun, B. Yan, C. Felser, N. Avraham, and H. Beidenkopf, Fermi-arc diversity on surface terminations of the magnetic Weyl semimetal $\text{Co}_3\text{Sn}_2\text{S}_2$, *Science* **365**, 1286 (2019).